Photon statistics as a probe for exciton correlations in coupled nanostructures

A. Carmele,* A. Knorr, and M. Richter
Institut für Theoretische Physik, Nichtlineare Optik und Quantenelektronik, Technische Universität Berlin, Hardenbergstr. 36, 10623 Berlin, Germany

(Received 28 November 2008; published 15 January 2009)

Quantum light excitation of Coulomb-coupled nanostructures, such as semiconductor quantum dots or light harvesting molecules, is analyzed for fixed light intensity but different photon statistics. The theory predicts a different excitation efficiency of the exciting light (thermal, coherent, and squeezed light) on the creation of optically active excitons and biexcitons. In particular, measurable differences and a strong dependence for the creation efficiency of biexcitons on the photon statistics are obtained.

DOI: 10.1103/PhysRevB.79.035316 PACS number(s): 78.67.Hc, 42.50.Ar, 73.21.La, 78.47.N−

I. INTRODUCTION

Excitonic excitations in Coulomb-coupled nanostructures are of particular interest to understand many basic processes in many particle physics. Important examples are light harvesting complexes in coupled photosynthetical units[1] and nanoscale energy transfer in metal structures as well as semiconducting nanocrystals[2] or in polymer composites.[3] Manmade system for promising applications, such as entangled photon processing,[4–6] are coupled semiconductor nanostructures,[7] since their size, shape, composition, and location can be controlled by modern epitaxial growth techniques[8] or chemical synthesis.[9] In our analysis, we focus on dipole-dipole-coupled nanostructures such as semiconductor quantum dots, providing typical couplings and parameters, representative for many of the mentioned nanosystems.

In this paper, we focus on Coulomb coupling via dipole-dipole interaction, which leads to energy renormalization of the ground, exciton, and biexciton states and Förster coupling. These interactions transform the isolated two-level systems into a multilevel system.[10] Thus, the coupled quantum systems form new eigenstates and the individual systems cannot be excited separately: excitons and many exciton states, such as biexcitons, are formed.[11] Our goal is to consider the fully quantized electron-light interaction in a multilevel system, expanding previous semiclassical investigations on the nonlinear response of exciton-exciton correlations.[12] We evaluate the impact of photon statistics of the incident light on the creation of excitons and biexcitons using the photon statistics of the excitation light as an additional parameter to differentiate between these many particle excitations and presenting hereby a theoretical approach to implement photon-statistical properties[13] in coupled semiconductor structures.

The statistical properties of the exciting light source can be determined by the Hanbury Brown and Twiss[14] experiment and designed, e.g., using emission from a quantum dot ensemble in a high-$\mathcal{Q}$ optical microcavity.[15] Addressing the quantum-optical properties of the excitation light, we calculate the electron-light interaction on a microscopic level.[16,17] Self-consistently including photon-statistical and Coulomb effects we predict a measurable and strong impact of the light source on the creation of biexcitons in comparison to the creation of single excitons.

We focus on the excitation with thermal, coherent, and squeezed light. Even if all parameters are chosen for Coulomb-coupled quantum dots,[18] all results reported here apply also to other coupled nanostructures in which Coulomb couplings are of primary importance. We expand the investigations of isolated atoms interacting with a quantized light field[19–21] and translationally invariant semiconductors[16] to Coulomb-coupled nanostructures. For instance, to give an important example, photosynthetical units such as the light harvesting complex II of green plants[22] can be described as Förster-coupled chlorophyll molecules[23] and they interact with thermal sunlight, approximated by the photon statistics of black body radiation.

II. PHOTON STATISTICS

To characterize photon statistics of the excitation light source, one typically uses the Hanbury Brown and Twiss[14] setup, which is illustrated in Fig. 1. It consists of a light source, a beam splitter, two photon detectors, and a correlator. In this setup one measures the second-order correlation function of two intensities at measurement time t (detector 1) and $t+\tau$ (detector 2), defining τ as the delay time

$$g^{(2)}(t,\tau) = \frac{\langle :I(t)I(t+\tau):\rangle}{\langle I(t)\rangle\langle I(t+\tau)\rangle}, \tag{1}$$

which represents the normalized deviation from a Poisson distribution.[24] We discuss three typical cases for $g^{(2)}$ [(i)–(iii)]. (i) If there is no correlation between the emitted photons, the $g^{(2)}$ of a Poisson distribution has the value 1. The probability to measure a photon at the detector 2 is indepen-

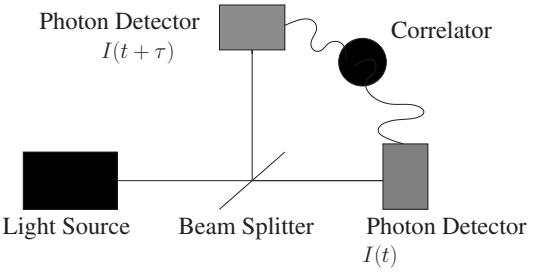

FIG. 1. Hanbury Brown and Twiss (Ref. 14) experiment.

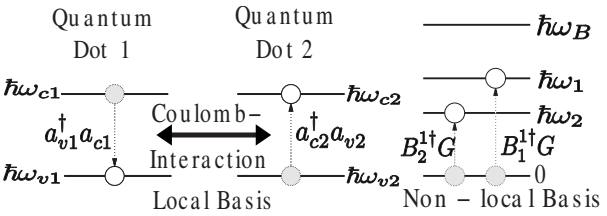

FIG. 2. Local (electron operators $a^{(\dagger)}$) and nonlocal (exciton operator $B^{(\dagger)}$) excitation schemes of two Coulomb-coupled quantum dots. Förster interaction transforms the coupled two-level systems into a four-level system.

dent of the measurement result at detector 1. Examples for this photon statistics are laser fields well above threshold, representing coherent (Glauber) states.[25] (ii) If it is more probable to measure a photon at detector 2, after detector 1 has measured a photon, the light field is described via a super-Poissonian statistics, showing photon bunching. An example is a thermal light field, which shows $g^{(2)}=2$. An example is the Bose-Einstein distribution of the black body radiation.[24] (iii) The light field is in a sub-Poissonian state if $g^{(2)}$ is smaller than 1, meaning it is less probable to measure a photon at detector 2 after a positive measurement result at detector 1 is registered. This effect is called antibunching. An example is squeezed light emitted by a single-photon emitter.[26]

III. COUPLED EXCITON SYSTEM

Starting in a local basis (see Fig. 2), the total Hamiltonian $H_{\text{local}}=H_{0e}+H_{e\text{-}e}+H_{0p}+H_{e\text{-}p}$ is expressed via local annihilation (creation) operators and includes the free energy of the electronic H_{0e} and photonic system H_{0p}, the electron-electron interaction $H_{e\text{-}e}$, and the electron-light interaction $H_{e\text{-}p}$. The free-energy part of the electronic system reads

$$H_{0e}=\sum_n (\hbar\omega_{vn}a_{vn}^\dagger a_{vn}+\hbar\omega_{cn}a_{cn}^\dagger a_{cn}). \tag{2}$$

The electronic states of Coulomb-coupled quantum dots are described via local annihilation (creation) operators $a_{in}^{(\dagger)}$, where i denotes the electronic state and $n=(1,2)$ the quantum dot. Each quantum dot has one valence and one conduction-band state in effective-mass approximation of each individual nanostructure,[27] thus $i=(v,c)$ with $\hbar\omega_{vn}$ valence band and $\hbar\omega_{cn}$ conduction-band energy of quantum dot n. The number of electrons is conserved inside every quantum dot, i.e., tunneling between the quantum dots is prohibited.

The two-particle interaction Hamiltonian $H_{e\text{-}e}$ describes the Coulomb interaction and can be expressed in the local basis of creation and annihilation operator of the individual dots[10,28]

$$\begin{aligned}H_{e\text{-}e}=&V_F a_{c1}^\dagger a_{v2}^\dagger a_{c2}a_{v1}+V_F^* a_{v1}^\dagger a_{c2}^\dagger a_{v2}a_{c1}+V_{cv}a_{c1}^\dagger a_{v2}^\dagger a_{v2}a_{c1}\\&+V_{vc}a_{v1}^\dagger a_{c2}^\dagger a_{c2}a_{v1}+V_{cc}a_{c1}^\dagger a_{c2}^\dagger a_{c2}a_{c1}+V_{vv}a_{v1}^\dagger a_{v2}^\dagger a_{v2}a_{v1}.\end{aligned} \tag{3}$$

The Coulomb-interaction results in a ground-state shift V_{vv}, two monoexciton shifts V_{vc}^{12}, V_{cv}^{21}, and a biexciton shift V_{cc}. These shifts correspond to energy renormalizations caused by electrostatic interactions. V_F^{12} describes a nonradiative Coulomb energy transfer from one quantum dot to the other. H_{0e} and $H_{e\text{-}e}$ can be written in terms of four two-electron operators by defining $G=a_{v1}^\dagger a_{v2}^\dagger a_{v2}a_{v1}$ as the ground-state operator, $P_1^1=a_{v1}^\dagger a_{v2}^\dagger a_{v2}a_{c1}$ and $P_2^1=a_{v1}^\dagger a_{v2}^\dagger a_{c2}a_{v1}$ as single-polarization operators leading to an annihilation of a single-excitonic state, and $P^2=a_{v1}^\dagger a_{v2}^\dagger a_{c2}a_{c1}$ as the double-polarization operator, leading to an annihilation of a biexcitonic state. In this local two-electron basis,[23] the Hamiltonian of the electronic system $H_e=H_{0e}+H_{e\text{-}e}$ has nondiagonal contribution due to the Förster-coupling V_F,

$$H_e=\begin{pmatrix}A&0&0&0\\0&B&V_F^*&0\\0&V_F&C&0\\0&0&0&D\end{pmatrix}, \tag{4}$$

with $A=\hbar\omega_{v1}+\hbar\omega_{v2}+V_{vv}$, $B=\hbar\omega_{v2}+\hbar\omega_{c1}+V_{vc}$, $C=\hbar\omega_{v1}+\hbar\omega_{c2}+V_{cv}$, and $D=\hbar\omega_{c1}+\hbar\omega_{c2}+V_{cc}$.

Thus, taking Förster coupling into account,[11] P_1^1 and P_2^1 are no longer eigenstates of the Hamiltonian [see Eq. (4)]. To find the new eigenstates, the electron part of the Hamiltonian is diagonalized[23] and the local basis illustrated in Fig. 2 is transformed into the nonlocal exciton basis: in our case into a four-level system. All Coulomb-induced energy shifts are included in the definition of the new operators derived via diagonalization (ground state, monoexcitonic, and biexcitonic shifts and Förster interaction). New collective operators are formed: $G^{(\dagger)}$ is the ground state, $B^{2(\dagger)}$ the biexciton annihilation (creation) operator, replacing two-particle operators $a_{v1}^\dagger a_{v2}^\dagger a_{c2}a_{c1}$, and $B_m^{1(\dagger)}$ the exciton annihilation (creation) operator $(m=1,2)$. Within the nonlocal basis the electron operators $(G^{(\dagger)},B_m^{1(\dagger)},B^{2(\dagger)})$ are eigenvectors of the electron part of the Hamiltonian with eigenvalues $(\hbar\omega_G,\hbar\omega_m,\hbar\omega_B)$. $B_m^{1(\dagger)}$ represent a superposition of localized polarizations[23]

$$B_m^1=\sum_n v_n^m P_n^1. \tag{5}$$

The coefficients v_n^m depend on the strength of the Förster coupling, the energy of the monoexcitonic energy shifts, and on the band-gap frequencies. In case of two coupled quantum dots, they can be calculated analytically via the quantity $\Delta_e=V_F(B-\hbar\omega_1)^{-1}=-V_F(C-\hbar\omega_2)^{-1}$:

$$v_1^1=-v_2^2=-(1+\Delta_e^2)^{-1/2}\Delta_e, \tag{6}$$

$$v_2^1=v_1^2=(1+\Delta_e^2)^{-1/2}. \tag{7}$$

The electron-light interaction (matrix element M_{kn}^{vc}) is also transformed into the new basis.[23] Starting from the local two-electron basis, $H_{e\text{-}p}$ reads in a rotating-wave approximation[27]

$$H_{e\text{-}p}=-\sum_{\substack{k,n\\m\neq n}} M_{kn}^{vc}(G^\dagger P_n^1 c_k^\dagger+P_m^{1\dagger}P^2 c_k^\dagger)+\text{H.c.}, \tag{8}$$

where $c_k^{(\dagger)}$ denotes the Boson annihilation (creation) operator of the photon in the excitation and dissipation modes with

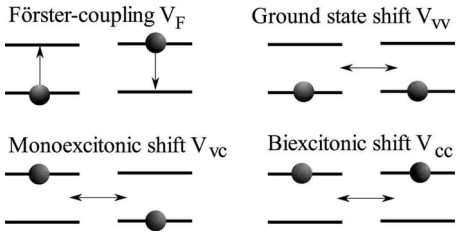

FIG. 3. Coulomb-interaction between the electrons leads to energy renormalization of the ground state V_{vv}, monoexcitonic V_{vc}, and biexcitonic state V_{cc}, as well as to Förster coupling V_F, corresponding to a nonradiative energy transfer between the quantum dots.

frequency $\omega=ck$ and m and n the quantum dots (Fig. 3). Equation (8) incorporates radiative coupling between the dots, as well as local electron-light interaction. Using Eq. (5) and introducing nonlocal matrix elements $(\bar{M}_m^k, \bar{M}_{m,2}^k)$, $H_{e\text{-}p}$ is expressed via nonlocal electron operators. The nonlocal matrix elements are defined as[23]

$$\bar{M}_m^k = \sum_n (v_n^m)^* \bar{M}_{kn}^{vc}, \tag{9}$$

$$\bar{M}_{m,2}^k = \sum_{i,n\neq i} v_n^m \bar{M}_{ki}^{vc}. \tag{10}$$

The new matrix elements include important characteristics of Förster-coupled systems, e.g., a vanishing electron-light interaction (dark states) in the case of two identical systems (quantum dots).[10] Since the free-energy Hamiltonian of the photonic system H_{0p} stays unchanged, the total Hamiltonian of the diagonalized system reads

$$H = \sum_m \hbar\omega_m B_m^{1\dagger} B_m^1 + \hbar\omega_B B^{2\dagger} B^2 + \sum_k \hbar\omega_k c_k^\dagger c_k - \hbar \sum_{km} (\bar{M}_m^k G^\dagger B_m^1 c_k^\dagger + \bar{M}_{m,2}^k B_m^{1\dagger} B^2 c_k^\dagger) + \text{H.c.} \tag{11}$$

The ground-state energy is chosen to be zero and $\hbar\omega_m$ and $\hbar\omega_B$ denote the energy levels of the four-level system, illustrated in Fig. 2, with two exciton and one biexciton levels.

IV. EQUATIONS OF MOTION

The temporal evolution of the system is calculated via the Heisenberg equation of motion $-i\hbar\partial_t A=[H,A]$ for occurring many-body expectation values (see below). We focus on $\langle A\rangle=\{\langle B_1^{1\dagger}B_1^1\rangle, \langle B_2^{1\dagger}B_2^1\rangle, \langle B^{2\dagger}B^2\rangle\}$ as observable quantities; Fig. 4 depicts the corresponding excitation scheme. All correlations up to the fourth order of the light-coupling element $\bar{M}_m^k$ are included. The corresponding set of equations reads for single-mode excitation, i.e., $c_k^{(\dagger)} \equiv c^{(\dagger)}$ (with $\bar{M}_m^k = \bar{M}_m$). Also, to consider dissipation processes, the electronic system is coupled to a photon reservoir, which causes a decay of the exciton and biexciton states.[24] The decay rate is described via the Einstein coefficient $\Gamma=(500\ \text{ps})^{-1}$.[10] The equations for the ground state and excited-state densities read

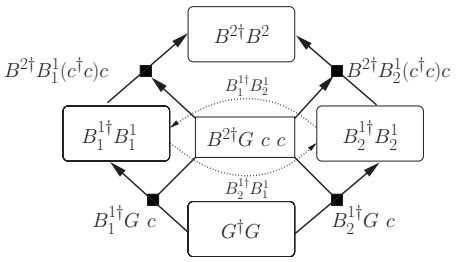

FIG. 4. Excitation scheme for two Coulomb-coupled quantum dots. $G^{(\dagger)}$ is the ground state, $B_m^{1(\dagger)}$ the exciton, and $B^{2(\dagger)}$ the biexciton annihilation (creation) operator. To create a biexciton density, there are three excitation paths. The two-photon polarization $B^{2\dagger}Gcc$ is crucial for the photon statistics and couples to the photon-density-assisted exciton-biexciton polarizations $B^{2\dagger}B_m^1 c^\dagger cc$ $(m=1,2)$.

$$\partial_t\langle G^\dagger G\rangle = 2\Gamma(\langle B_1^{1\dagger}B_1^1\rangle + \langle B_2^{1\dagger}B_2^1\rangle) - 2\sum_m \text{Im}(\bar{M}_m\langle G^\dagger B_m^1 c^\dagger\rangle), \tag{12}$$

$$\partial_t\langle B_m^{1\dagger}B_m^1\rangle = -2\Gamma(\langle B_m^{1\dagger}B_m^1\rangle - \langle B^{2\dagger}B^2\rangle) + 2\,\text{Im}(\bar{M}_{m,2}^*\langle B^{2\dagger}B_m^1 c\rangle + \bar{M}_m\langle G^\dagger B_m^1 c^\dagger\rangle), \tag{13}$$

$$\partial_t\langle B^{2\dagger}B^2\rangle = -4\Gamma\langle B^{2\dagger}B^2\rangle + 2\sum_m \text{Im}(\bar{M}_{m,2}\langle B_m^{1\dagger}B^2 c^\dagger\rangle). \tag{14}$$

The electronic densities in Eqs. (12)–(14) couple to photon-assisted polarizations. The photon-assisted polarizations in the second order of electron-light coupling read

$$\partial_t\langle G^\dagger B_m^1 c^\dagger\rangle = -i(\omega_m-\omega-i\Gamma)\langle G^\dagger B_m^1 c^\dagger\rangle + i(\bar{M}_m^*\langle G^\dagger G c^\dagger c\rangle + \bar{M}_{m,2}\langle G^\dagger B^2 c^\dagger c^\dagger\rangle) - i\sum_l \bar{M}_l^*(\langle B_l^{1\dagger}B_m^1 c^\dagger c\rangle + \langle B_l^{1\dagger}B_m^1\rangle), \tag{15}$$

$$\partial_t\langle B_m^{1\dagger}B^2 c^\dagger\rangle = -i(\omega_B-\omega_m-\omega-3i\Gamma)\langle B_m^{1\dagger}B^2 c^\dagger\rangle - i(\bar{M}_{m,2}^*\langle B^{2\dagger}B^2 c^\dagger c\rangle + \bar{M}_{m,2}^*\langle B^{2\dagger}B^2\rangle) - i\bar{M}_m\langle G^\dagger B^2 c^\dagger c^\dagger\rangle + i\sum_l \bar{M}_{l,2}^*\langle B_m^{1\dagger}B_l^1 c^\dagger c\rangle. \tag{16}$$

A Born approximation in this order of electron-light coupling element leads to a photon-density-driven inversion. Since the intensity of the driving field is expressed via the photon density and is chosen to be equal for different light sources, differences in the photon statistics do not enter in the present order of electron-light coupling element. Equations (15) and (16) include spontaneous emission and couple to photon-assisted densities, which are given in the Appendix [Eqs. (A2) and (A3)]. A characteristic quantity of Förster-coupled nanostructures is a two-photon polarization $\langle G^\dagger B^2 c^\dagger c^\dagger\rangle$, which enters in higher order photon-assisted polarization [see Fig. 4 and Eq. (A5)]

$$\partial_t\langle G^\dagger B_n^1 c^\dagger c^\dagger c\rangle = -i(\omega_n^1 - \omega - i\Gamma)\langle G^\dagger B_m^1 c^\dagger c^\dagger c\rangle - 2i\sum_l \bar{M}_l^*\langle B_l^{1\dagger} B_n^1 c^\dagger c\rangle - i\sum_l \bar{M}_l^*\langle B_l^{1\dagger} B_n^1 c^\dagger c^\dagger cc\rangle - i\bar{M}_n^*\langle G^\dagger G c^\dagger c^\dagger cc\rangle + i\bar{M}_{n,2}\langle G^\dagger B^2 c^\dagger c^\dagger c^\dagger c\rangle + i\bar{M}_{n,2}\langle G^\dagger B^2 c^\dagger c^\dagger\rangle, \tag{17}$$

$$\partial_t\langle B_m^{1\dagger} B^2 c^\dagger c^\dagger c\rangle = -i(\omega^2 - \omega_m^1 - \omega - 3i\Gamma)\langle B_m^{1\dagger} B^2 c^\dagger c^\dagger c\rangle - 2i\bar{M}_{m,2}^*\langle B^{2\dagger} B^2 c^\dagger c\rangle - i\bar{M}_{m,2}^*\langle B^{2\dagger} B^2 c^\dagger c^\dagger cc\rangle + i\sum_l \bar{M}_{l,2}^*\langle B_m^{1\dagger} B_l^1 c^\dagger c^\dagger cc\rangle - i\bar{M}_m\langle G^\dagger B^2 c^\dagger c^\dagger c^\dagger c\rangle. \tag{18}$$

On this level, also the photon statistics of the incident radiation occurs via its characteristic $g^{(2)}$ value, including bunching or antibunching features (cf. Sec. II). In the fourth order of the light-coupling element, the set of differential equations is closed via the Born approximation[29] $\langle B_1^{1\dagger} B_1^1 c^\dagger c^\dagger cc\rangle = \langle B_1^{1\dagger} B_1^1\rangle\langle c^\dagger c^\dagger cc\rangle$. Here, the photon correlation $\langle c^\dagger c^\dagger cc\rangle$ is represented by $g^{(2)} = \langle c^\dagger c^\dagger cc\rangle / \langle c^\dagger c\rangle^2$ [see Eq. (1)]; replacing $\langle c^\dagger c^\dagger cc\rangle$ with $g^{(2)}\langle c^\dagger c\rangle^2$ statistical properties is implemented via the choice of $g^{(2)}$. After these approximations, substitution, and neglecting quantities, which couple to fifth order in the light coupling, hence Eqs. (18) and (17) read

$$\partial_t\langle G^\dagger B_n^1 c^\dagger c^\dagger c\rangle = -i(\omega_n^1 - \omega - i\Gamma)\langle G^\dagger B_m^1 c^\dagger c^\dagger c\rangle - 2i\sum_l \bar{M}_l^*\langle B_l^{1\dagger} B_n^1 c^\dagger c\rangle + i\bar{M}_n^* g^{(2)}\langle c^\dagger c\rangle^2\langle G^\dagger G\rangle - i\sum_l \bar{M}_l^* g^{(2)}\langle c^\dagger c\rangle^2\langle B_l^{1\dagger} B_n^1\rangle + i\bar{M}_{n,2}\langle G^\dagger B^2 c^\dagger c^\dagger\rangle, \tag{19}$$

$$\partial_t\langle B_m^{1\dagger} B^2 c^\dagger c^\dagger c\rangle = -i(\omega^2 - \omega_m^1 - \omega - 3i\Gamma)\langle B_m^{1\dagger} B^2 c^\dagger c^\dagger c\rangle - 2i\bar{M}_{m,2}^*\langle B^{2\dagger} B^2 c^\dagger c\rangle - i\bar{M}_{m,2}^* g^{(2)}\langle c^\dagger c\rangle^2 \times\langle B^{2\dagger} B^2\rangle + i\sum_l \bar{M}_{l,2}^* g^{(2)}\langle c^\dagger c\rangle^2\langle B_m^{1\dagger} B_l^1\rangle. \tag{20}$$

The set of differential equations is closed. In Eqs. (19) and (20), typical quantum-optical effects are visible such as the spontaneous emission, depending in the fourth order only on photon-density-assisted exciton and biexciton densities. Also the photon-density-driven inversion, responsible for induced-absorption and emission processes, can be recognized. Furthermore, characteristic for Förster-coupled nanostructures, excitation transfer from, e.g., quantum dot L to quantum n influences the system dynamics.

V. NUMERICAL RESULTS

The system of differential equations [Eqs. (14)–(18)] is numerically solved. Initially, the electronic system is in the ground state $\langle G^\dagger G\rangle = 1$; all other quantities are zero. Light sources with different $g^{(2)}$, but having an equal mean photon number $\langle c^\dagger c\rangle$ are chosen to discuss the $g^{(2)}$ dependence of the excitation efficiency. The $g^{(2)}$ function differs in the case of $\tau = 0$ for different statistics (thermal light: $g^{(2)} = 2$, coherent light: $g^{(2)} = 1$, squeezed light: $g^{(2)} = 0.2$).[30] Since we have a single mode theory, the stationary excitation of a constant flux of photons $\langle c^\dagger c\rangle$ balances the loss of photons due to spontaneous emission into the dissipative modes. The excitation strength is determined by the dipole moment M_m and photon number. It is kept within the validity of the applied Born approximation, which can be deduced by an independent evaluation of the Jaynes-Cummings model for a single exciton.[31] The excitation frequency is chosen to be resonant with one ground state to single-exciton transition [see Fig. 2], which is approximately half of the ground state to biexciton transition. Due to the Förster coupling, there is always an energy splitting between the exciton frequencies, so the exciton densities cannot be both in resonance (see Fig. 2 and the absorption spectrum, inset in Fig. 5). Figure 5 shows the exciton density of the lowest optical transition, the photon flux is adiabatically switched on. The optically generated exciton-density buildup is plotted for three values of $g^{(2)}$. The exciton density for squeezed and coherent excitations is higher than for thermal excitation. Thus, a small value for $g^{(2)}$ is advantageous if excitons are created. This occurs, since only one photon is absorbed to create an exciton and a part of the bunched photons passes the electronic system unused. In this case, it is more effective to excite with antibunched light when photons arrive successively. However, the quantitative influence of the photon statistics remains small. This changes drastically for the exciton of higher excitonic complexes. In Fig. 6 the biexciton density for different $g^{(2)}$ is plotted. Here, thermal excitation is clearly advantageous for creating biexciton densities. The influence of the photon statistics has an opposite effect compared with excitonic excitations: biexciton creation is a two-photon process, thus more susceptible to photon correlations. Compared to the single-exciton dynamics in Fig. 5, where antibunched light is advantageous for the creation of excitons, multiphoton processes, such as biexciton generation, e.g., $\langle B^{2\dagger} Gcc\rangle$ in Fig. 4, favor bunched photons, i.e., simultaneous absorption of photon pairs. Therefore, biexcitonic levels are populated stronger for thermal excitation.

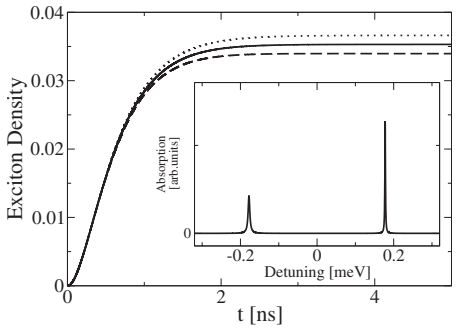

FIG. 5. Single-exciton dynamics for stationary excitation with different values for $g^{(2)}$. (Solid curve: $g^{(2)} = 1$, coherent excitation; dashed curve: $g^{(2)} = 2$, thermal excitation; dotted curve: $g^{(2)} = 0.2$, squeezed excitation.)

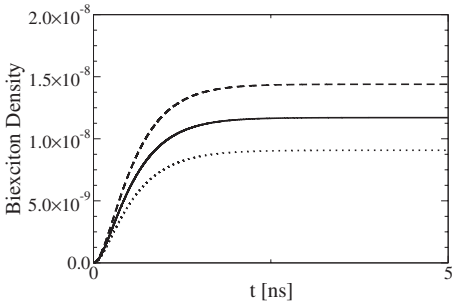

FIG. 6. Biexciton dynamics for stationary excitation with different values for $g^{(2)}$. (Solid curve: $g^{(2)}=1$, coherent excitation; dashed curve: thermal excitation $g^{(2)}=2$; dotted curve: squeezed excitation $g^{(2)}=0.2$).

Next, we study the excitation dependence of the quantum-optical excitation scheme. In Fig. 7, the exciton densities are plotted as a function of the excitation strength $\langle c^\dagger c\rangle = n$ (mean photon number). Also the percental deviation from coherent (laser $g^{(2)}=1$) defined by

$$\Delta B^1_{\mathrm{th/sq}} = \frac{\langle B^{1\dagger}_m B^1_m\rangle_{\mathrm{coh}} - \langle B^{1\dagger}_m B^1_m\rangle_{\mathrm{th/sq}}}{\langle B^{1\dagger}_m B^1_m\rangle_{\mathrm{coh}}} \times 100 \qquad (21)$$

is shown. The exciton-density deviation depends linearly on the mean photon number of the photon flux. For weak pumping, the photon-statistical impact on the creation of single excitons can be neglected. The calculations confirm that for single-excitons different values of $g^{(2)}$ are negligible, unless the excitation strength is high enough to populate many-particle correlations $\langle G^\dagger B^{1\dagger}_m c^\dagger c^\dagger c\rangle$, $\langle B^{1\dagger}_m B^2 c^\dagger c^\dagger c\rangle$ in the fourth order of the light-coupling element. With increasing excitation strength, the difference becomes measurable in a typical pump-probe experiment.[17,27] In our case, the theory predicts differences up to 3% (not shown). For comparison, in Fig. 8, the more sensitive biexciton densities and its deviation from coherent excitation (ΔB^2) are plotted

$$\Delta B^2_{\mathrm{th/sq}} = \frac{\langle B^{2\dagger} B^2\rangle_{\mathrm{coh}} - \langle B^{2\dagger} B^2\rangle_{\mathrm{th/sq}}}{\langle B^{2\dagger} B^2\rangle_{\mathrm{coh}}} \times 100. \qquad (22)$$

Here, photon statistics show a large impact: up to 40% deviation in populating the biexciton density can be obtained rather independently of the excitation strength. Furthermore,

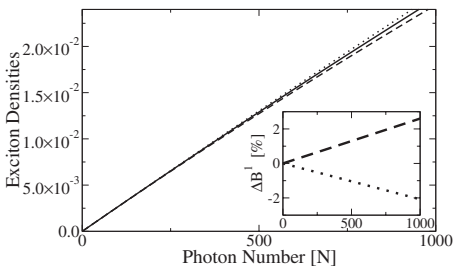

FIG. 7. Exciton density and percental exciton-density differences as a function of the excitation strength. The coherently driven exciton density (solid curve) is taken as a benchmark (dashed curve: ΔB^1_{th} for thermal excitation; dotted curve: ΔB^1_{sq} for squeezed excitation).

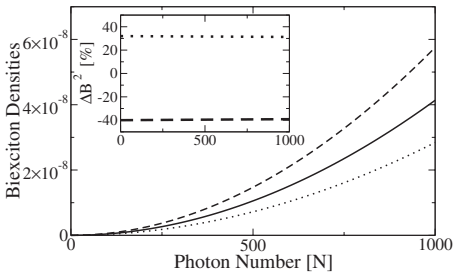

FIG. 8. Biexciton density and percental biexciton density differences as a function of the excitation strength. The coherently driven biexciton density (solid curve) is taken as a benchmark (dashed curve: ΔB^2_{th} for thermal excitation; dotted curve: ΔB^2_{sq} for squeezed excitation).

a qualitative change cf. to Fig. 7 can be seen; thermal excitation populates biexcitons stronger, thus the deviation is negative, in contrast to the case when creation of single excitons is investigated and deviation is positive, showing an inversed behavior with respect to exciton generation. With higher excitation strength only the absolute value of the deviation increases, but not the relative.

VI. CONCLUSION

In conclusion, our results suggest strong qualitative differences of excitonic and biexcitonic behaviors on the photon statistics of the incident light. The photon statistics takes advantage of different aspects of the material excitation and may be used for possible optical device, detecting absorption of different many particle species to measure the photon statistics directly.

ACKNOWLEDGMENT

We acknowledge support from the Deutsche Forschungsgemeinschaft (DFG).

APPENDIX: EQUATIONS OF MOTION

In Förster-coupled nanostructures, exciton transfer occurs. The equation of motion reads

$$\partial_t\langle B^{1\dagger}_m B^1_n\rangle = -i(\omega_n-\omega_m-2i\Gamma)\langle B^{1\dagger}_m B^1_n\rangle - i(\bar{M}^*_{m,2}\langle B^{2\dagger}B^1_n c\rangle - \bar{M}_{n,2}\langle B^{1\dagger}_m B^2 c^\dagger\rangle) - i(\bar{M}_m\langle G^\dagger B^1_n c^\dagger\rangle - \bar{M}^*_n\langle B^{1\dagger}_m G c\rangle). \qquad (A1)$$

This quantity depends strongly on the energy splitting, thus on the Coulomb parameter. It oscillates for strong Förster coupling and is driven by the photon-assisted polarizations, which couple to photon-assisted exciton densities

$$\partial_t\langle G^\dagger G c^\dagger c\rangle = 2\Gamma(\langle B^{1\dagger}_1 B^1_1 c^\dagger c\rangle + \langle B^{1\dagger}_2 B^1_2 c^\dagger c\rangle) - 2\sum_m \mathrm{Im}(\bar{M}_m\langle G^\dagger B^1_m c^\dagger\rangle) - 2\sum_m \mathrm{Im}(\bar{M}_m\langle G^\dagger B^1_m c^\dagger c^\dagger c\rangle), \qquad (A2)$$

$$\partial_t\langle B^{2\dagger}B^2c^\dagger c\rangle = -4\Gamma\langle B^{2\dagger}B^2c^\dagger c\rangle + 2\sum_m \mathrm{Im}(\bar{M}_{m,2}\langle B_m^{1\dagger}B^2c^\dagger c^\dagger c\rangle), \tag{A3}$$

$$\begin{aligned}\partial_t\langle B_m^{1\dagger}B_n^1c^\dagger c\rangle = &-i(\omega_n^1-\omega_m^1-2i\Gamma)\langle B_m^{1\dagger}B_n^1c^\dagger c\rangle\\ &-i(\bar{M}_m\langle G^\dagger B_n^1c^\dagger c^\dagger c\rangle-\bar{M}_n^*\langle B_m^{1\dagger}Gc^\dagger cc\rangle)\\ &-i(\bar{M}_{m,2}^*\langle B^{2\dagger}B_n^1c^\dagger cc\rangle-\bar{M}_{n,2}\langle B_m^{1\dagger}B^2c^\dagger c^\dagger c\rangle)\\ &-i(\bar{M}_{m,2}^*\langle B^{2\dagger}B_n^1c\rangle-\bar{M}_{n,2}\langle B_m^{1\dagger}B^2c^\dagger\rangle).\end{aligned} \tag{A4}$$

These photon-assisted exciton densities decay with the Einstein coefficient Γ exactly like the exciton densities. The third order in the electron-light coupling element $\bar{M}_m$ couples to the fourth order, which as well includes the two-photon polarization

$$\begin{aligned}\partial_t\langle G^\dagger B^2c^\dagger c^\dagger\rangle = &-i(\omega_B-2\omega-2i\Gamma)\langle G^\dagger B^2c^\dagger c^\dagger\rangle\\ &-i\sum_m \bar{M}_m^*(2\langle B_m^{1\dagger}B^2c^\dagger\rangle+\langle B_m^{1\dagger}B^2c^\dagger c^\dagger c\rangle)\\ &+i\sum_m \bar{M}_{m,2}^*\langle G^\dagger B_m^1c^\dagger c^\dagger c\rangle.\end{aligned} \tag{A5}$$

The two-photon polarization opens two additional channels to excite a biexciton in the coupled system. Due to this quantity, which influences the quantitative results strongly, a simple analytical solution cannot be derived.

*alex@itp.physik.tu-berlin.de

[1] T. Renger and R. A. Marcus, J. Chem. Phys. **116**, 9997 (2002).
[2] A. O. Govorov, J. Lee, and N. A. Kotov, Phys. Rev. B **76**, 125308 (2007).
[3] M. Anni, L. Manna, R. Cingolani, D. Valerini, A. Cretí, and M. Lomascolo, Appl. Phys. Lett. **85**, 4169 (2004).
[4] U. Hohenester, G. Pfanner, and M. Seliger, Phys. Rev. Lett. **99**, 047402 (2007).
[5] R. M. Stevenson, R. Young, P. Atkinson, K. Cooper, D. Ritchie, and A. Shields, Nature (London) **439**, 179 (2006).
[6] N. Akopian, N. H. Lindner, E. Poem, Y. Berlatzky, J. Avron, D. Gershoni, B. D. Gerardot, and P. M. Petroff, Phys. Rev. Lett. **96**, 130501 (2006).
[7] S. Stufler, P. Machnikowski, P. Ester, M. Bichler, V. M. Axt, T. Kuhn, and A. Zrenner, Phys. Rev. B **73**, 125304 (2006).
[8] D. Bimberg, M. Grundmann, and N. N. Ledentsov, *Quantum Dot Heterostructures* (Wiley, Chichester, 1999).
[9] B. O. Dabbousi, J. Rodriguez-Viejo, F. V. Mikulec, J. R. Heine, H. Mattoussi, R. Ober, K. F. Jensen, and M. G. Bawendi, J. Phys. Chem. B **101**, 9463 (1997).
[10] J. Danckwerts, K. J. Ahn, J. Förstner, and A. Knorr, Phys. Rev. B **73**, 165318 (2006).
[11] T. Unold, K. Mueller, C. Lienau, T. Elsaesser, and A. D. Wieck, Phys. Rev. Lett. **94**, 137404 (2005).
[12] T. Ostreich, K. Schonhammer, and L. J. Sham, Phys. Rev. B **58**, 12920 (1998).
[13] M. Kira and S. W. Koch, Phys. Rev. A **78**, 022102 (2008).
[14] R. Hanbury Brown and R. Twiss, Nature (London) **177**, 27 (1956).
[15] C. Gies, J. Wiersig, M. Lorke, and F. Jahnke, Phys. Rev. A **75**, 013803 (2007).
[16] M. Kira and S. W. Koch, Phys. Rev. A **73**, 013813 (2006).
[17] T. Altevogt, H. Puff, and R. Zimmermann, Phys. Rev. A **56**, 1592 (1997).
[18] $E_{\mathrm{gap}}=1.4$ eV; $V_F=1$ meV Förster interaction; $V_{cc}=V_{vc}=0.1$ meV for biexciton and single-exciton shifts; $d_{vc}=0.3$ e nm for the dipole moment.
[19] A. S. Parkins, Phys. Rev. A **53**, 2893 (1996).
[20] J. Gea-Banacloche, Phys. Rev. Lett. **62**, 1603 (1989).
[21] N. P. Georgiades, E. S. Polzik, and H. J. Kimble, Phys. Rev. A **59**, 676 (1999).
[22] M. Richter, T. Renger, G. Renger, and A. Knorr, J. Chem. Phys. **127**, 075105 (2007a).
[23] M. Richter, K. J. Ahn, A. Knorr, A. Schliwa, D. Bimberg, M. E.-A. Madjet, and T. Renger, Phys. Status Solidi B **243**, 2302 (2006).
[24] L. Mandel and E. Wolf, *Optical Coherence and Quantum Optics* (Cambridge University Press, Cambridge, 1995).
[25] R. Glauber, Phys. Rev. **130**, 2529 (1963).
[26] G. J. Beirne, P. Michler, M. Jetter, and H. Schweizer, J. Appl. Phys. **98**, 093522 (2005).
[27] H. Haug and S. W. Koch, *Quantum Theory of the Optical and Electronic Properties of Semiconductors* (World Scientific, Singapore, 2004).
[28] M. Richter, T. Renger, and A. Knorr, Photosynth. Res. **95**, 119 (2008).
[29] M. Richter, S. Butscher, M. Schaarschmidt, and A. Knorr, Phys. Rev. B **75**, 115331 (2007b).
[30] S. M. Ulrich, C. Gies, S. Ates, J. Wiersig, S. Reitzenstein, C. Hofmann, A. Löffler, A. Forchel, F. Jahnke, and P. Michler, Phys. Rev. Lett. **98**, 043906 (2007).
[31] E. Jaynes and F. Cummings, Proc. IEEE **51**, 89 (1963).